(He^3,α) Reactions from Nickel and Zirconium Isotopes*

D. E. Rundquist,† M. K. Brussel, and A. I. Yavin
Department of Physics, University of Illinois, Urbana, Illinois
(Received 19 June 1967)

The stable isotopes of nickel and zirconium, with the exception of Zr^{96}, have been irradiated with a 25-MeV He^3 beam. Absolute cross sections for (He^3,α) reactions have been measured. The (He^3,α) angular distributions for l transfers of 1 and 3 were found to contain some J-dependent effects, especially in the lighter isotopes of nickel. Distorted-wave Born-approximation (DWBA) predictions for all of the measured angular distributions are presented. Corrections for finite-range nonlocal potential were included in the DWBA calculations by use of the local-energy approximation. Spectroscopic factors were extracted. Some discussion on the merits of the (He^3,α) reaction as a general nuclear spectroscopic tool is presented.

I. INTRODUCTION

THE motivation for the present experiment was twofold: (1) to investigate the (He^3,α) reaction as a possible spectroscopic tool in nuclear structure studies; (2) to obtain spectroscopic information about the elements involved in the study.

The use of the (He^3,α) reaction as a spectroscopic tool to investigate nuclear structure offers several advantages. Experimentally, the detected α-particle groups are easily identified, because the Q value for these reactions is usually large (approximately +10 MeV for nickel and zirconium targets). In addition, neutron-pickup reactions [(p,d), (d,t), and (He^3,α)] provide the best direct means for the study of certain isotopes, such as Ni^{57} and Zr^{89}. (He^3,α) reactions, however, differ from (p,d) or (d,t) reactions in that they favor transitions which involve higher orbital angular-momentum transfers.[1] This is important in the study of the Ni and Zr isotopes, since, in a shell-model description, the last full neutron shell in Ni is $f_{7/2}$, and the last full neutron shell in Zr is $g_{9/2}$. The (He^3,α) reaction should therefore be particularly effective in studying neutron pickup from these shells.

Ni and Zr isotopes have been investigated by several laboratories[2–8] in recent years, primarily via (d,p) and (d,t) reactions. Some (He^3,α) reactions,[1,7,9] mostly at low-beam energies, and (α,He^3) reactions[8] have also been reported.

The experimental procedure and apparatus have been previously discussed.[10,11] In Sec. II we present the experimental results. Section III gives a brief outline of DWBA theory as applied to the present experiment. Section IV presents the DWBA analysis as applied to the individual transitions. Our summary and conclusions are contained in Sec. V.

II. EXPERIMENTAL RESULTS

A. Experimental Procedure

Figures 1 and 2 show spectra from Ni^{62} and Zr^{90} targets. These spectra are seen to be dominated by the He^3 elastic-scattering peaks, which were always a few orders of magnitude larger than the α peaks. The largest of the α peaks in each spectrum usually corresponded to the pickup of an $f_{7/2}$ neutron in Ni and a $g_{9/2}$ neutron in Zr. The beam energy was nominally 25 MeV. The energy resolution of the data depended on the target thickness and the beam intensity. A typical resolution was 140 keV. The smallest beam-energy spread was roughly 100 keV, indicating that the incident beam was the major factor in the energy resolution.

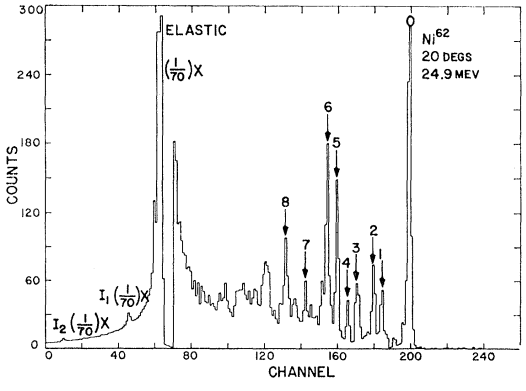

FIG. 1. Spectrum from Ni^{62} at the lab scattering angle of 20 deg. Peak heights were reduced by the factor of 70 for all channels lower than channel 70.

* Supported in part by the U. S. Office of Naval Research.
† Present address: Department of Physics, University of Michigan, Ann Arbor, Mich.

[1] A. G. Blair and H. E. Wegner, Phys. Rev. **127**, 1233 (1962).
[2] R. H. Fulmer, A. L. McCarthy, B. L. Cohen, and R. Middleton, Phys. Rev. **133**, B955 (1964).
[3] R. H. Fulmer and W. W. Daehnick, Phys. Rev. **139**, B579 (1965).
[4] B. L. Cohen and O. V. Chubinsky, Phys. Rev. **131**, 2184 (1963).
[5] E. R. Cosman, C. H. Paris, A. Sperduto, and H. A. Enge, Phys. Rev. **142**, 673 (1966).
[6] C. M. Fou and R. W. Zurmuhle, Phys. Rev. **140**, B1283 (1965).
[7] C. M. Fou, R. W. Zurmuhle, and L. S. Swenson, Phys. Rev. **144**, 927 (1966).
[8] C. R. Bingham, M. L. Halbert, and R. H. Bassel, Phys. Rev. **148**, 1174 (1966).
[9] W. Parker Alford, L. M. Blair, and D. Cline, Nucl. Phys. **61**, 368 (1965); D. Cline, L. M. Blair, and W. Parker Alford, *ibid.* **73**, 33 (1965); L. M. Blair, W. Parker Alford, D. Cline and H. E. Gove, *ibid.* **76**, 45 (1966).
[10] M. K. Brussel, D. E. Rundquist, and A. I. Yavin, Phys. Rev. **140**, B838 (1965).
[11] D. E. Rundquist, M. K. Brussel, and A. I. Yavin, preceding paper, Phys. Rev. **168**, 1287 (1968).

Our experimental excitation energies for the peaks observed are tabulated in Tables I–IX. The first column refers to an assigned peak number for each isotope, and the second column refers to the corresponding excitation energy of the respective residual nucleus. The other tabulated quantities will be discussed below. The estimated accuracy of the quoted excitation energies is ±40 keV (possibly slightly higher for levels with a large excitation energy).

Some of the observed peaks correspond to several resolved levels which have previously been seen in higher resolution studies. This does not necessarily render these data useless, since an unresolved group of

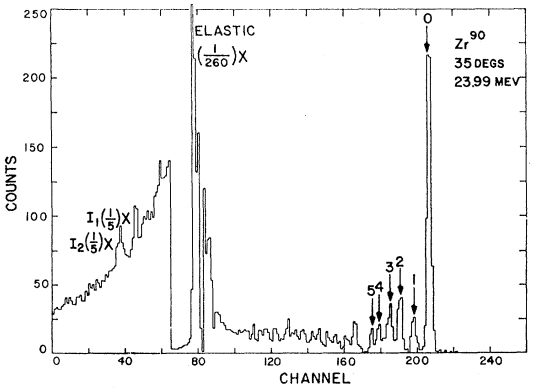

FIG. 2. Spectrum from Zr^{90} at the lab scattering angle of 35 deg. Peak heights were reduced by a factor of 5 for all channels below channel 65. The elastic peak is reduced by a factor of 260.

TABLE I. Excitation energy, orbital angular momentum, total angular momentum, and spectroscopic factors for the observed $Ni^{58}(He^3,\alpha)Ni^{57}$ transitions.

Peak No.	Excitation energy (MeV)	l	J	S
0	0.0	1	$\frac{3}{2}$	1.08
1	0.76	3	$\frac{5}{2}$	0.86
2	1.08	1	$\frac{1}{2}$	0.13
3	2.58	3	$\frac{7}{2}$	2.59
4	3.26	3	$\frac{7}{2}$	0.69
5	3.83	3	$\frac{7}{2}$	0.43
6	4.26	3	$\frac{7}{2}$	0.37
7	4.59	3	$\frac{7}{2}$	0.45
8	5.28	3	$\frac{7}{2}$	2.41
10	6.12	3	$\frac{7}{2}$	0.91

TABLE II. Excitation energy, orbital angular momentum, total angular momentum, and spectroscopic factors for the observed $Ni^{60}(He^3,\alpha)Ni^{59}$ transitions.

Peak No.	Excitation energy (MeV)	l	J	S
0	0.0	1	$\frac{3}{2}$	1.72
1	0.35	3	$\frac{5}{2}$	1.61
2	0.87	1	$\frac{3}{2}$	0.18
3	1.33	1	$\frac{1}{2}$	0.18
4	1.70	3	$\frac{5}{2}$	0.14
5	1.96	3	$\frac{7}{2}$	0.42
6	2.67	3	$\frac{7}{2}$	1.18
7	3.10	3	$\frac{7}{2}$	0.68

TABLE III. Excitation energy, orbital angular momentum, total angular momentum, and spectroscopic factors for the observed $Ni^{61}(He^3,\alpha)Ni^{60}$ transitions. Parentheses indicate either tentative assignment or an unresolved group.

Peak No.	Excitation energy (MeV)	l	J	S
0	0.0	1	0	0.35
1	1.33	1	2	0.40
2	2.20	3	2	1.71
3	2.59	(3)	···	0.43
4	3.20	(3)	···	0.91
8	6.15	(3)	···	0.72

TABLE IV. Excitation energy, orbital angular momentum, total angular momentum, and spectroscopic factors for the observed $Ni^{62}(He^3,\alpha)Ni^{61}$ transitions. Parentheses indicate either tentative assignment or an unresolved group.

Peak No.	Excitation energy (MeV)	l	J	S
0	0.07	(1)	$(\frac{3}{2})$	···
		(3)	$(\frac{5}{2})$	(3.03)
1	1.15	(1)	$(\frac{3}{2})$	···
		(3)	$(\frac{5}{2})$	(0.59)
2	1.45	3	$\frac{7}{2}$	0.47
3	2.10	(4)	$(\frac{9}{2})$	(0.27)
4	2.47	3	$(\frac{5}{2})$	0.23
5	2.90	3	$\frac{7}{2}$	0.60
6	3.31	3	$\frac{7}{2}$	0.91
8	4.94	(3)	$(\frac{7}{2})$	(0.69)

TABLE V. Excitation energy, orbital angular momentum, total angular momentum, and spectroscopic factors for the observed $Ni^{64}(He^3,\alpha)Ni^{63}$ transitions. Parentheses indicate either tentative assignment or an unresolved group.

Peak No.	Excitation energy (MeV)	l	J	S
0	0.10	3	$\frac{5}{2}$	(3.23)
1	0.52	1	$\frac{3}{2}$	0.63
2	1.01	1	$(\frac{1}{2})$	0.30
3	1.29	4	$\frac{9}{2}$	0.32
5	2.14	1	$\frac{1}{2}$	0.55
6	2.53	4	$\frac{9}{2}$	0.19
7	3.55	3	$\frac{7}{2}$	1.31
8	4.37	3	$\frac{7}{2}$	0.69

TABLE VI. Excitation energy, orbital angular momentum, total angular momentum, and spectroscopic factors for the observed $Zr^{90}(He^3,\alpha)Zr^{89}$ transitions. Parentheses indicate either tentative assignment or an unresolved group.

Peak No.	Excitation energy (MeV)	l	J	S
0	0.0	4	$\frac{9}{2}$	3.41
1	0.58	1	$(\frac{1}{2})$	2.07
2	1.08	1	$(\frac{3}{2})$	2.41
3	1.45	3	$(\frac{5}{2})$	2.59
4	1.82	3	$(\frac{5}{2})$	1.08

TABLE VII. Excitation energy, orbital angular momentum, total angular momentum, and spectroscopic factors for the observed $Zr^{91}(He^3,\alpha)Zr^{90}$ transitions. Parentheses indicate either tentative assignment or an unresolved group.

Peak No.	Excitation energy (MeV)	l	J	S
0	0.0	2	0	0.67
2	2.78	...	...	...
4	4.53	4	...	3.71
5	5.07	4	...	1.79

TABLE VIII. Excitation energy, orbital angular momentum, total angular momentum, and spectroscopic factors for the observed $Zr^{92}(He^3,\alpha)Zr^{90}$ transitions. Parentheses indicate either tentative assignment or an unresolved group.

Peak No.	Excitation energy (MeV)	l	J	S
0	0.0	2	$\frac{5}{2}$	0.86
1	2.14	4	$\frac{7}{2}$	0.36
2	2.90	...	...	...
3	3.54	(4)	$(\frac{7}{2})$	(0.68)
4	3.89	4	$\frac{9}{2}$	0.71

TABLE IX. Excitation energy, orbital angular momentum, total angular momentum, and spectroscopic factors for the observed $Zr^{94}(He^3,\alpha)Zr^{93}$ transitions. Parentheses indicate either tentative assignment or an unresolved group.

Peak No.	Excitation energy (MeV)	l	J	S
0	0.0	2	$\frac{5}{2}$	2.16
1	1.49	(2)	$(\frac{3}{2})$	(0.33)
2	2.05	4	$\frac{7}{2}$	0.31
3	3.14	4	$\frac{9}{2}$	1.21
4	3.83	4	$\frac{9}{2}$	0.75

two peaks often combines levels that correspond to orbital angular-momentum transfers which are either equal or differ by two units (1 and 3 in Ni and 2 and 4 in Zr). Because (He^3,α) reactions favor the higher value of the l transfer, the excitation strength of the level with the smaller l value is strongly inhibited. In fact, the contribution from the level with the smaller l transfer can often be neglected.

The observed (He^3,α) angular distributions are plotted in Figs. 3–11. DWBA fits to the experimental data (discussed below) are also plotted in the figures. Note that the experimental angular distributions have the typical direct interaction characteristics of large cross sections at forward angles, an exponential falloff, and usually a diffractionlike structure. Error flags represent mostly the statistical uncertainty.

Data were taken at scattering angles up to 90 deg in the laboratory coordinate system. A few preliminary runs in Ni^{58} and Ni^{60} were attempted at 110, 120, and 160 deg. These runs were only of an exploratory nature, but were sufficient to show that the cross section at backward angles was prohibitively low.

B. Characteristics of the Angular Distributions

The ground states of Ni and Zr isotopes are described, to a first approximation, as having full neutron and proton shells with only a few excess neutrons outside the closed shells. For Ni this means that in a neutron pickup reaction a neutron is picked up from $p_{3/2}$, $p_{1/2}$, and $f_{5/2}$ outer shells or the closed $f_{7/2}$ shell. We therefore expected to see primarily states which correspond to an l transfer of 1 or 3. In Zr, the shells of importance are the $d_{5/2}$, $d_{3/2}$, and $g_{7/2}$ outer shells and the closed $g_{9/2}$ shell. Here we expected to see primarily l transfers of 2 and 4.

For the (He^3,α) reaction to be of value as a spectroscopic tool, it is at least necessary to be able to determine orbital angular-momentum transfers. For instance, the curves labeled 0 (g.s.) and 3 (2.58 MeV) in Fig. 3 illustrate angular distributions for known l transfers of 1 and 3, respectively. The identifying characteristic of $l=1$ transitions is readily apparent from the observed angular distribution. The structure of the angular distribution is much more pronounced for $l=1$ than for $l=3$ transitions. In general, we found $l=3$ transitions to have very little structure in the angular distribution. The situation in Zr is less straightforward. The lack of a distinct structure in the (He^3,α) angular distribution in Zr makes the identification of the orbital angular-momentum transfer difficult. However, the angular distributions for the transitions to the ground states of Zr^{90}, Zr^{91}, and Zr^{93} do display some oscillatory structure. These transitions correspond to the pickup of a $d_{5/2}$ neutron.[4] This might be taken as some evidence, though inconclusive, that the shapes of the $l=2$ and $l=4$ angular distributions are different. Another criterion for the differentiation between $l=2$ and $l=4$ angular distributions was also tried. We normalized the angular distributions by dividing each of them by the same decreasing exponential, $e^{-K\theta}$. When these normalized cross sections are plotted, it appears that the $l=4$ curves usually fall off more rapidly with increasing scattering angle (Figs. 12–16). The two criteria were used to suggest l whenever such information was not previously available. A few examples will now be presented, and a more complete discussion will be deferred for a later section.

Normalized angular distributions for all of the observed $Zr^{94}(He^3,\alpha)Zr^{93}$ transitions are plotted on a semilogarithmic scale as a function of the c.m. scattering angle in Fig. 11. The factor K in the exponential is the same for each of the plotted curves. There is no apparent distinctive characteristic to the curves. However, curves 2, 3, and 4 appear to have a slightly different average slope from that for 0 and 1. This effect is best seen for the strongly excited state, No. 3, which has an average slope that is significantly different from that of 0 or 1. Since curve zero [ground state (g.s.) transition] corresponds to $l=2$, we suggest that curves 2, 3, and 4 correspond to $l=4$.

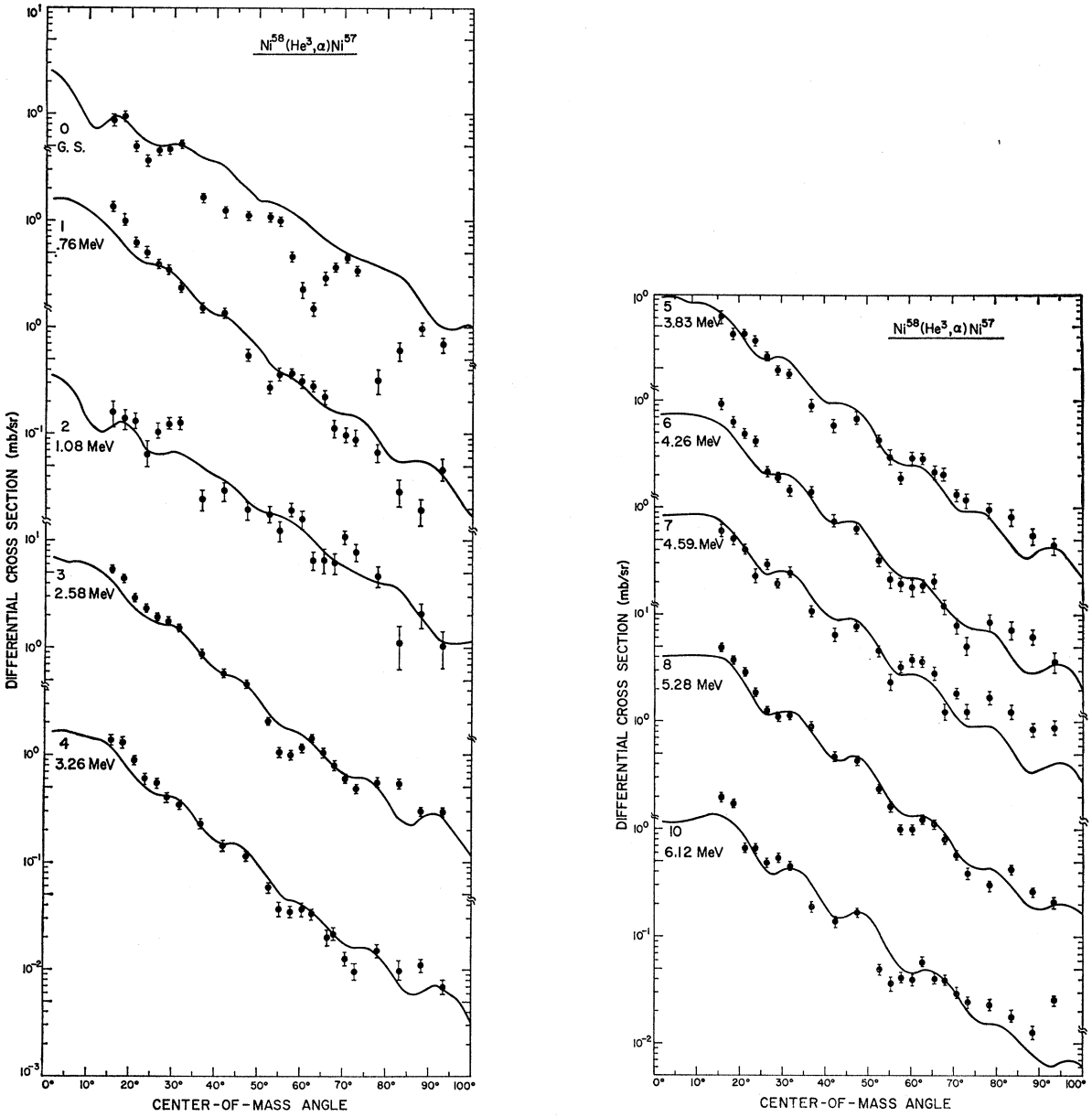

FIG. 3. Angular distributions for $Ni^{58}(He^3,\alpha)Ni^{57}$ reactions. The smooth curves represent DWBA fits to the data. The number refers to the peak number in the energy spectra. The excitation energy of each state is also given.

Figure 12 contains a similar plot for all of the experimentally determined $Zr^{90}(He^3,\alpha)Zr^{89}$ angular distributions. Other work[12] has determined an orbital angular-momentum transfer of $l=4$ for the g. s. transition (curve 0), $l=1$ for the next two transitions (curves 1 and 2), and $l=3$ for the fourth transition (curve 3). Curve 0 of Fig. 12 has the only nonpositive average slope; curves 3 and 4 are similar to each other and have a slightly positive average slope; the plots for curves 1 and 2 are also similar to each other with a more positive average slope than 3 and 4, particularly at the forward angles. Our results thus suggest that the average slope of the angular distribution depends on l. Moreover, these results indicate that for Zr, as the l transfer increases, the average slope of the angular distribution decreases. This effect holds for all of the Zr angular distributions, and is particularly noticeable for those states which are well resolved or strongly excited.

The normalization procedure of plotting the ratio of the differential cross section to an exponential is also expected to emphasize any oscillatory structure that exists in the angular distribution. With the exception

[12] C. M. Fou, R. W. Zurmuhle, and J. M. Joyce, Bull. Am. Phys. Soc. 11, 333 (1966).

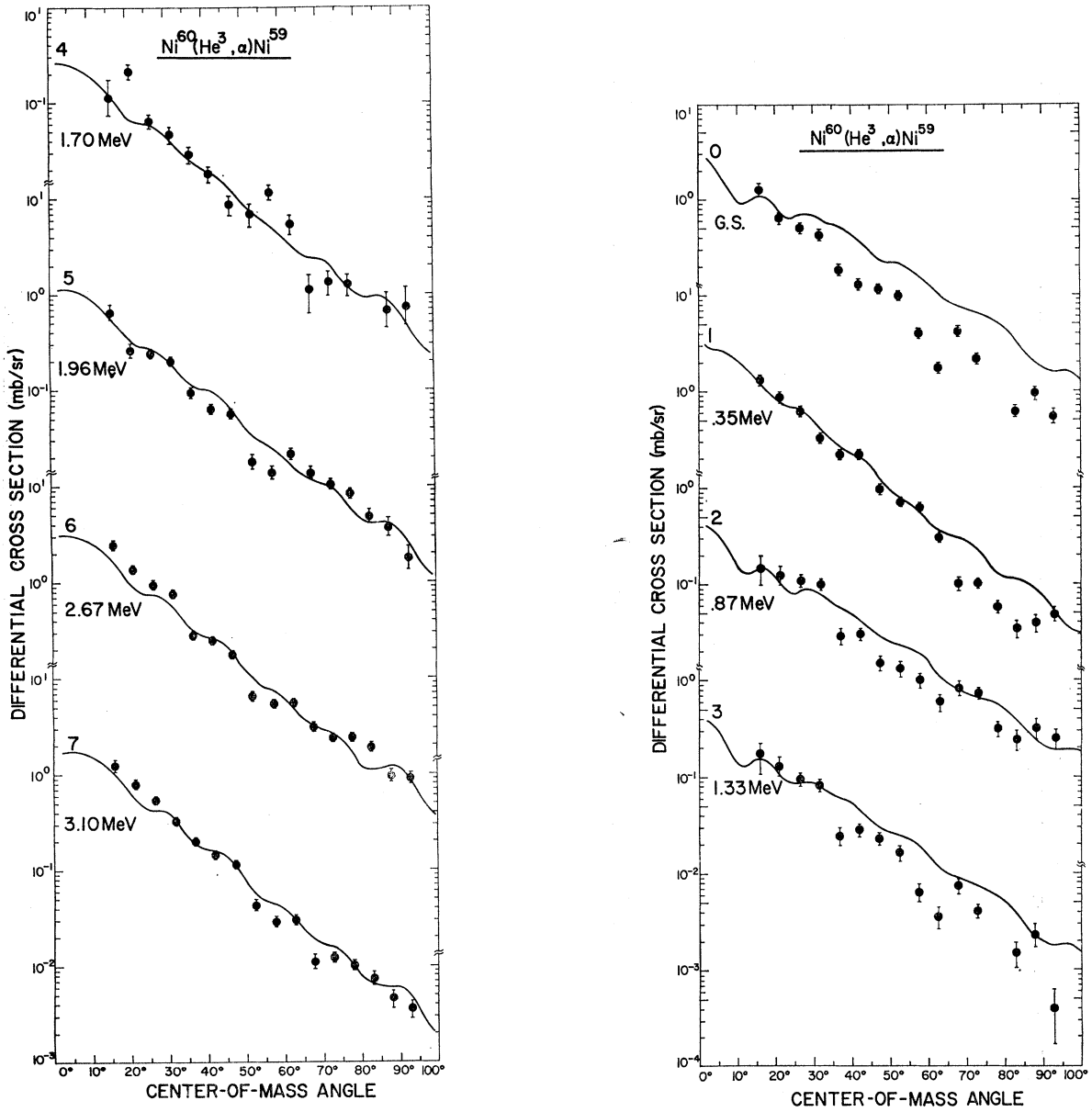

FIG. 4. Angular distributions for $Ni^{60}(He^3,\alpha)Ni^{59}$ reactions. See caption for Fig. 3.

of the $d_{5/2}$ transitions mentioned above, no well-defined structure was revealed in any of the $Zr(He^3,\alpha)$ angular distributions.

For Ni the ratio plots emphasize the structure that was observed in the angular distribution. Ratios for all of the Ni^{58} and Ni^{60} data are plotted in Fig. 14. The curves for the $l=1$ transitions (curves 0 and 2) for the $Ni^{58}(He^3,\alpha)Ni^{57}$ reaction, and (curves 0, 2, and 3) for the $Ni^{60}(He^3,\alpha)Ni^{59}$ reaction, have a more pronounced structure than the $l=3$ curves. These differences between the $l=1$ and $l=3$ transitions are already apparent without taking the ratios of the angular distributions, but the normalized plots reveal more subtle differences in the angular distributions.

C. *J* Dependence

In a previous paper[10] we discussed the J dependence of (He^3,α) reactions. The more complete study of the data is basically consistent with our previous conclusions. That is, for $l=1$ transitions the $J=\frac{3}{2}$ angular distributions seem to exhibit a more pronounced structure than the $J=\frac{1}{2}$ angular distributions. For $l=3$ transitions, the angular positions of the peaks and valleys of the $J=\frac{5}{2}$ distributions are approximately 5 deg forward relative to the corresponding peaks and valleys of the $J=\frac{7}{2}$ distribution. The ratio plots emphasize these properties as shown in Fig. 15 ($l=1$) and Fig. 16 ($l=3$). No J dependence for transitions with $l=2$ and $l=4$ could be observed.

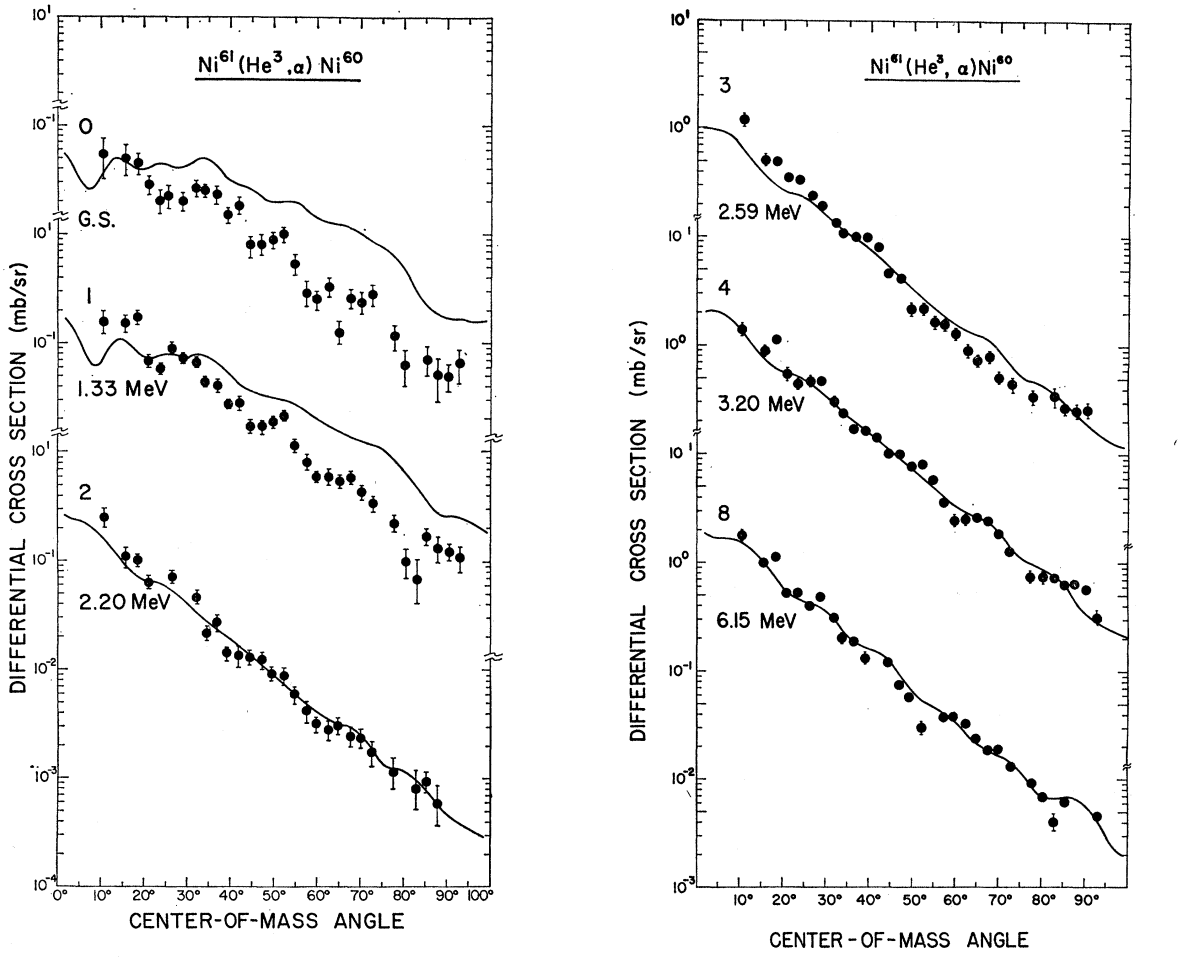

FIG. 5. Angular distributions for $Ni^{61}(He^3,\alpha)Ni^{60}$ reactions. See caption for Fig. 3.

III. DWBA THEORY AS APPLIED TO PICKUP REACTIONS

The general equations (1) and (2) of the preceding paper[11] apply to pickup reactions as well as inelastic scattering. However, the distorted-wave function for the exit channel in pickup reactions describes the elastic scattering of the outgoing particle from the final nucleus.

In a general pickup reaction $A(a,b)B$, it is convenient to consider the outgoing particle b as composed of the incoming particle a and the transferred particle x: $b=a+x$. [For a (He^3,α) reaction, a represents the He^3 particle, x is the picked-up neutron, and b is the outgoing α particle.] DWBA theory[13] assumes that the potential responsible for the rearrangement collision is V_{ax}. [In a (He^3,α) reaction, this is the potential $V_{He^3,n}$ between the incoming He^3 particle and the picked-up neutron, in a relative s state.] Explicitly, the matrix element taken between the internal states of the colliding nuclides is given by[14]

$$\langle\psi_b\psi_B|V|\psi_a\psi_A\rangle=\int\psi_{J_BM_B}{}^*(\zeta_B)\times\psi_{S_BM_B}{}^*(\mathbf{r}_{ax}\zeta_a\zeta_x)V_{ax}(\mathbf{r}_{ax}\zeta_a\zeta_x)\times\psi_{J_AM_A}(\mathbf{r}_{xB}\zeta_x\zeta_B)\psi_{S_aM_a}(\zeta_a)d\zeta_Bd\zeta_ad\zeta_x, \quad (1)$$

where ζ_I represents the internal coordinates of nucleus I.

Equation (1) may be evaluated when a parentage expansion is made. The zero-range approximation is usually also introduced at this point. Physically, this amounts to assuming that b is emitted from the same point at which a is absorbed. Mathematically, this amounts to replacing the product $V_{ax}(\mathbf{r}_{ax})\psi_b(\mathbf{r}_{ax})$ with a constant D_0, which denotes the strength of the interaction, and a δ function $\delta(\mathbf{r}_{ax})$. The "standard" DWBA calculations use the zero-range prescription with local potentials to evaluate the distorted-wave transition amplitude. This results in an expression containing a product of terms which includes the parentage co-

[13] G. R. Satchler, Argonne National Laboratory Report No. ANL-6878 (unpublished).

[14] G. R. Satchler, Nucl. Phys. 55, 1 (1964).

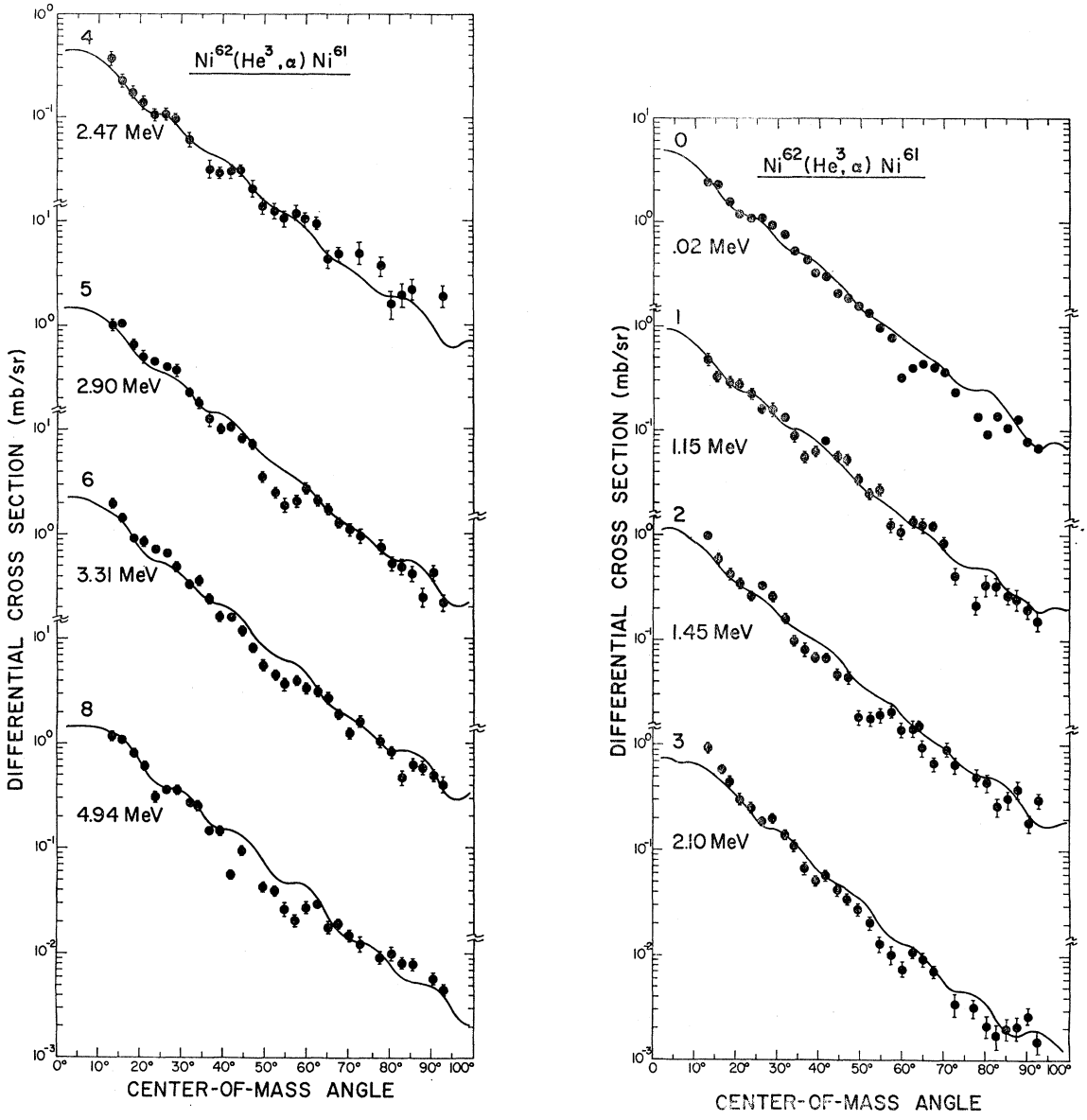

FIG. 6. Angular distributions for $Ni^{62}(He^3,\alpha)Ni^{61}$ reactions. See caption for Fig. 3.

efficient ($\alpha_{lj}{}^{AB}$), the strength of the interaction between x and a (D_0), the overlap of the internal states of b and x in the initial and final systems, and the bound-state wave function for the picked-up neutron [$u_l(r)$]. The bound-state wave function is normally determined by solving the Schrödinger equation for a particle having orbital angular momentum l in a Woods-Saxon potential well.

Finally, the differential cross section for a pickup reaction may be written in the form[9]

$$\frac{d\sigma}{d\Omega}(\theta)=\frac{2S_b+1}{2S_a+1}\frac{N}{2S_x+1}\sum_{lj}S(l,j)\bar{\sigma}_{lj}(\theta), \qquad (2)$$

where $\bar{\sigma}_{lj}(\theta)$ is the reduced cross section evaluated by the computer code for the pickup of a nucleon from the orbital state (l,j). The quantity $S(lj)$ is the spectroscopic factor

$$S(l,j)=n(\alpha_{lj}{}^{AB})^2, \qquad (3)$$

where n equals the number of equivalent nucleons in the (l,j) orbit of A. The factor N includes the effective overlap factor for $a+x$ and b as well as the strength of the interaction causing the transition.

The implications of the zero-range assumption for $V_{ax}\psi_b$ have been treated in detail by Austern *et al.*[15] They show that the approximation is most accurate in reactions which have a small momentum transfer or in

[15] N. Austern, R. Drisko, E. Halbert, and G. Satchler, Phys. Rev. 133, B3 (1964).

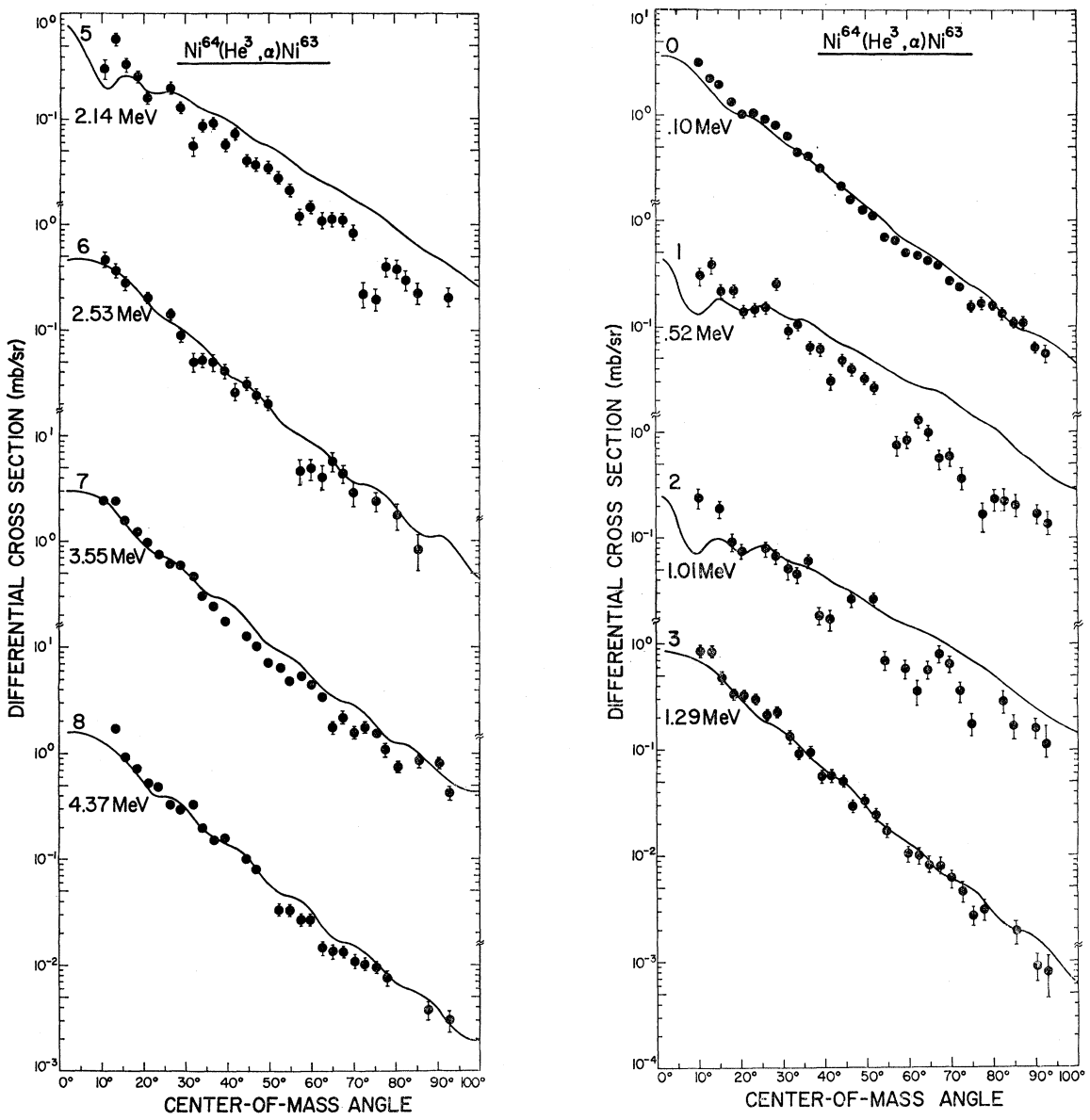

FIG. 7. Angular distributions for Ni^{64}(He^3,α)Ni^{63} reactions. See caption for Fig. 3.

inelastic scattering. The net effect of the zero-range approximation is to overemphasize possibly the importance of contributions to the cross section from the nuclear interior. This effect is the result of the δ function of the zero-range approximation which inhibits significant cancellations. These concellations might occur in the integral due to the oscillations of $\chi_{aA}^{(+)}$ and $\chi_{bB}^{(-)}$, the distorted wave functions for the initial and final channels, respectively.

Local potentials are utilized in the standard DWBA treatment. Perey and Sarius[16] have found that the use of nonlocal potentials tends to reduce the wave-function amplitude in the nuclear interior. Including nonlocality and finite-range exactly in a distorted-wave calculation is an extremely complicated and time consuming process. We have therefore used the "local energy approximation" (LEA),[17,18] which was developed in an attempt to correct the local potential, zero-range (L-ZR) theory in an approximate manner.

IV. DWBA ANALYSIS

The distorted-wave calculations for the pickup reactions were performed by the IBM 7090 code JULIE.[19] Ordinarily, this code utilizes the zero-range theory

[16] F. G. Perey and A. M. Sarius, Nucl. Phys. **70**, 225 (1965).

[17] F. G. Perey and D. Saxon, Phys. Letters **10**, 107 (1964).

[18] J. A. Buttle and L. J. B. Goldfarb, Proc. Phys. Soc. (London) **A83**, 701 (1964).

[19] Written by R. M. Drisko, Oak Ridge National Laboratory.

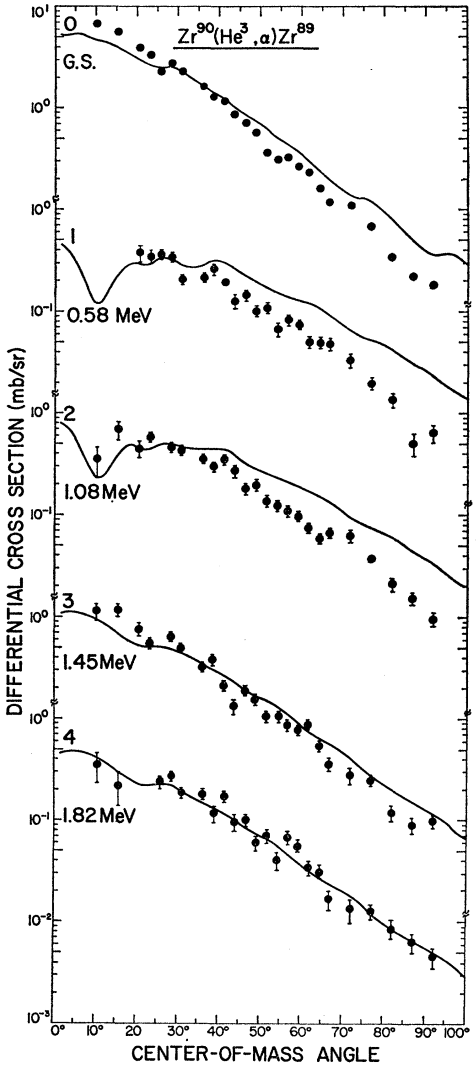

FIG. 8. $Zr^{90}(He^3,\alpha)Zr^{89}$ angular distributions. See caption for Fig. 3.

discussed in Sec. III. The code also contains an option for the inclusion of the bound-state wave function of the picked-up neutron. Corrections to the L-ZR theory may be fed into JULIE via this option.

The optical-model parameters for the (He^3,α) reaction, which were used for the entrance channel of the DWBA calculations, are discussed in the preceding paper.[11] The He^4 optical-model parameters for Ni were taken from a systematic analysis of 24.7-MeV α scattering by McFadden and Satchler.[20] Except for W_v, all of the parameters are the same as those in one of the parameter sets of McFadden and Satchler. W_v was determined by interpolating between the W_v results obtained for the 24.7-MeV incident α beam and those obtained at 43 MeV.[21] Since many parameter sets give equally good fits to the experimental data, the choice of the particular set listed in Table X was dictated by the desire to use the LEA.[22]

The optical parameters used for the calculations of (He^3,α) reactions in Zr were derived from 34.4-MeV α scattering on Zr^{90} targets. Ogata *et al.*[23] published results using a real well depth of 47.5 MeV. Since there is no experimental evidence that such a low well depth is necessary to describe α-particle scattering, we reanalyzed the data to find a parameter set with a real well depth near 200 MeV.

The bound-state wave function $u_l(r)$ was taken as the solution of Schrödinger's equation with a real Woods-Saxon potential. The radius parameter was 1.2 F, the diffusivity was 0.7 F, and the well depth was adjusted to give an eigenvalue equal to the binding energy. Spin-orbit coupling equal to 25 times the Thomas term was included. Since the elastic scattering data did not require a spin-orbit term in the optical-model analysis,

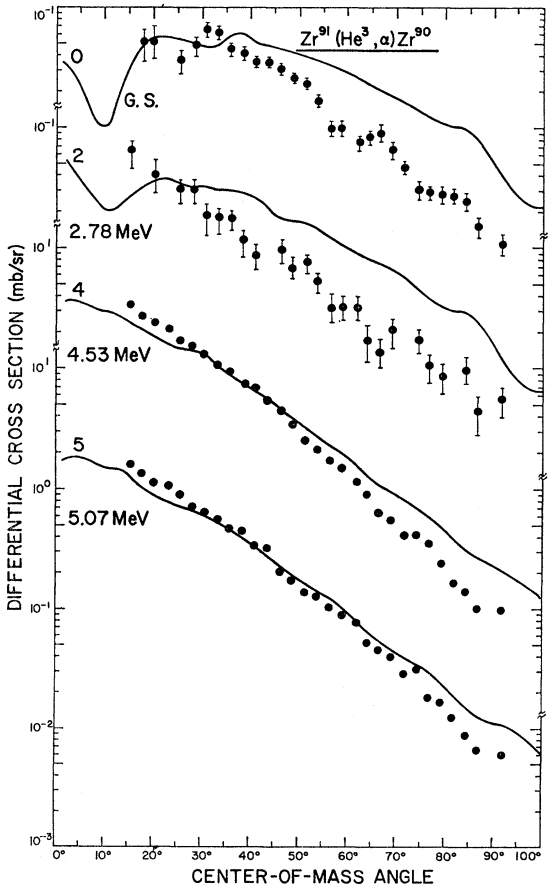

FIG. 9. $Zr^{91}(He^3,\alpha)Zr^{90}$ angular distributions. See caption for Fig. 3.

[20] L. McFadden and G. R. Satchler, Nucl. Phys. **84**, 177 (1966).
[21] G. R. Satchler (unpublished); data furnished by C. R. Bingham.
[22] J. K. Dickens, R. M. Drisko, F. G. Perey, and G. R. Satchler, Phys. Letters **15**, 337 (1965).
[23] H. Ogata, S. Tomita, M. Inone, Y. Okuma, and I. Kumabe, Phys. Letters **17**, 280 (1965).

no spin-orbit interaction was assumed for the entrance channel.

A few trial calculations using the L-ZR did not give satisfactory agreement with the experimental results and we therefore mostly used the LEA, for which finite-range and nonlocal corrections can be included without resorting to extremely lengthy computer calculations.

The program FANLFR2,[24] which uses the local-energy approximation, was available to calculate the bound-state wave function in any or all of the following options: (1) L-ZR; (2) nonlocal potential for the bound state, zero-range (NLBS-ZR); (3) nonlocal potential for the entrance and exit channels as well as the bound state, zero-range (NLALL-ZR); (4) nonlocal potential, finite-range (NLALL-FR). The form factor from this program was then read in as input to JULIE.

The predicted angular distributions for each of the four options are shown in Fig. 17 for the $Zr^{92}(He^3,\alpha)$ transitions to the g.s. ($l=2$) and to the second excited state at 2.90 MeV (assuming $l=4$) of Zr^{91}. The predicted

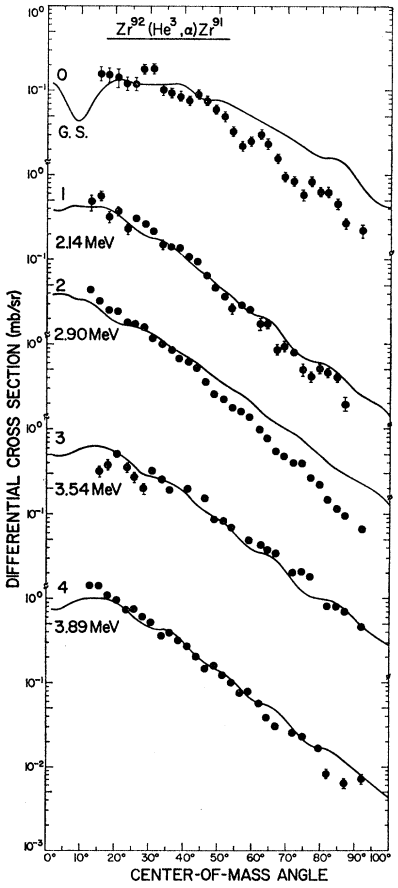

FIG. 10. $Zr^{92}(He^3,\alpha)Zr^{91}$ angular distributions. See caption for Fig. 3.

[24] Program written by J. K. Dickens, Oak Ridge National Laboratory.

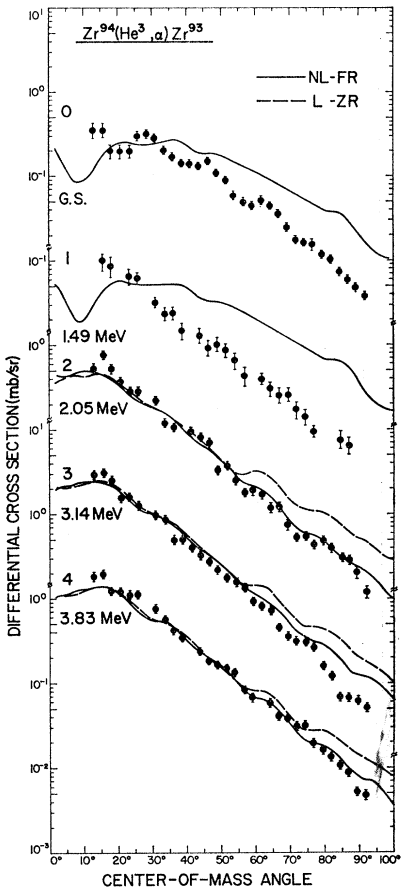

FIG. 11. $Zr^{94}(He^3,\alpha)Zr^{93}$ angular distributions. See caption for Fig. 3. The dashed curves are DWBA predictions using local potential, zero-range theory.

angular distributions for options 1, 2, and 3 are virtually indistinguishable in shape. It can be seen that the inclusion of the finite-range correction (option 4) slightly changes the predicted shape around 90 deg and the agreement here with the experimental curves is best. In view of these results, all of the distorted-wave analyses which follow, except where noted, have finite-range and nonlocal corrections included.

A limited attempt was made to determine the source of the J dependence observed in $l=1$ and $l=3$ angular distributions. The spin-orbit potential in the Schrödinger equation for the bound-state wave function is suggested as a possible source of J dependence. Distorted-wave calculations with the incorrect J (e.g., $J=\frac{7}{2}$ for an $l=3$ transition for which it is known that

TABLE X. He^4 optical parameters used for the exit channel of the (He^3,α) DWBA calculations.

	V_r (MeV)	r_r (F)	a_r (F)	W_v (MeV)	r_i (F)	a_i (F)	r_r (F)
Ni	198.6	1.458	0.502	24.7	1.458	0.502	1.4
Zr	193.5	1.39	0.563	21.41	1.39	0.563	1.4

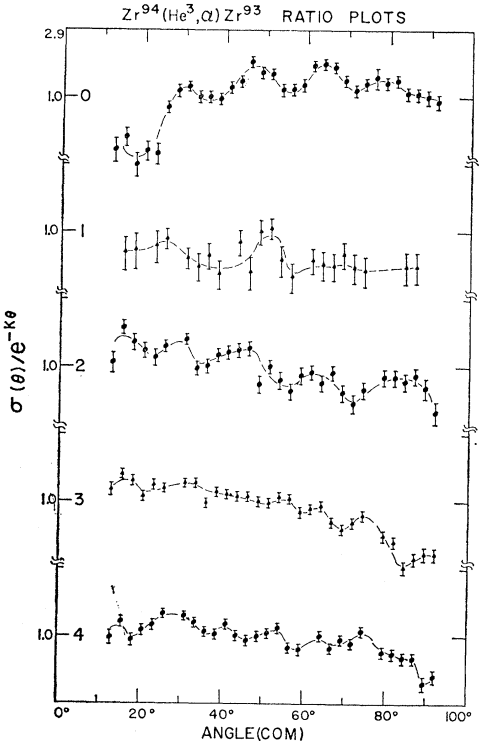

FIG. 12. Center-of-mass plots of the normalized $Zr^{94}(He^3,\alpha)Zr^{93}$ angular distribution. The dashed curves smoothly connect the points.

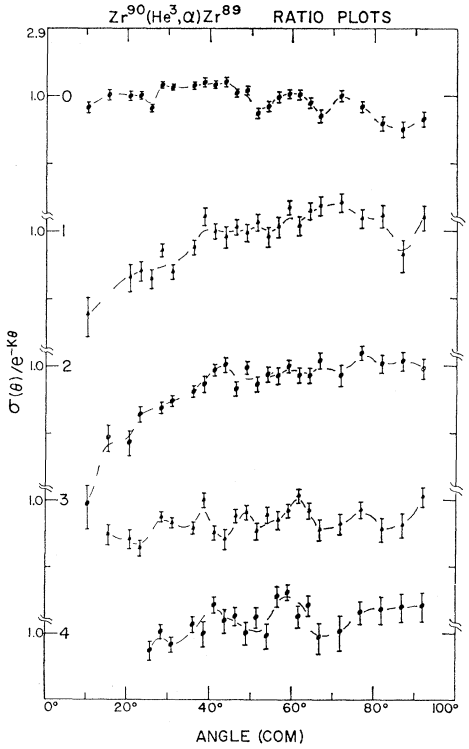

FIG. 13. Center-of-mass plots of the normalized $Zr^{90}(He^3,\alpha)Zr^{89}$ angular distribution. The dashed curves smoothly connect the points.

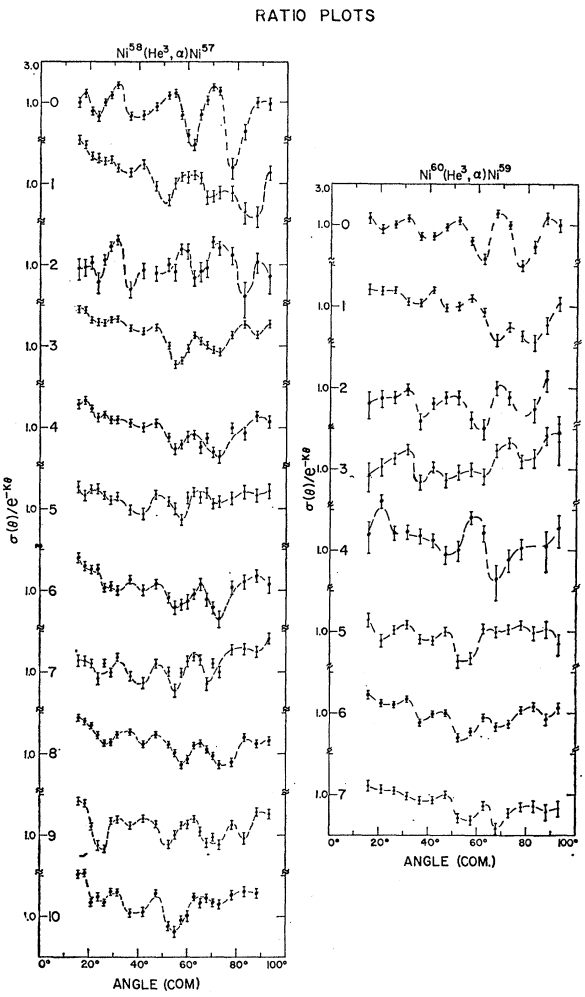

FIG. 14. Center-of-mass plots of the normalized $Ni^{58}(He^3,\alpha)Ni^{57}$ and $Ni^{60}(He^3,\alpha)Ni^{59}$ angular distribution. The dashed curves smoothly connect the points.

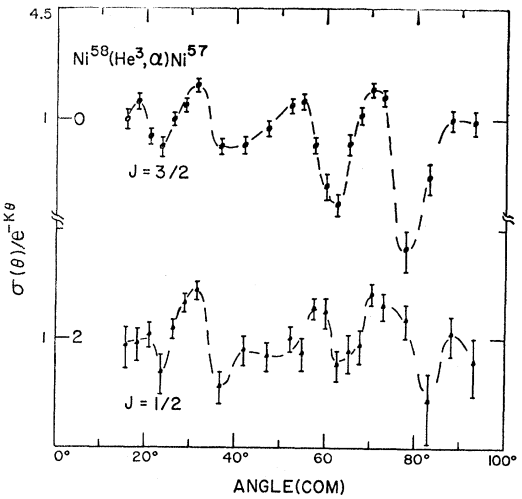

FIG. 15. Center-of-mass plots of the normalized $l=1$, $Ni^{58}(He^3,\alpha)Ni^{57}$ angular distribution. The dashed curves smoothly connect the points.

$J=\frac{5}{2}$) were tried. Computed angular distributions for the incorrect J are compared in Fig. 18 with the theoretical angular distributions having the correct J. The two predicted angular distributions for each of the four states considered are quite similar. Therefore, either the present DWBA calculations are not accurate enough to reproduce the observed J dependent effects or the source of the effects lies elsewhere.

If an accurate value of N in Eq. (2) is known, the absolute spectroscopic factor can be extracted by comparing Eq. (2) with the experimental differential cross section. In the present calculations, in which finite-range corrections have been included, no estimate of N has been made. Instead, the calculated cross sections were normalized to the experimental results by imposing a sum rule on the spectroscopic factors. Specifically, the spectroscopic factors for the first three states in Ni^{57} were required to add up to two, and the

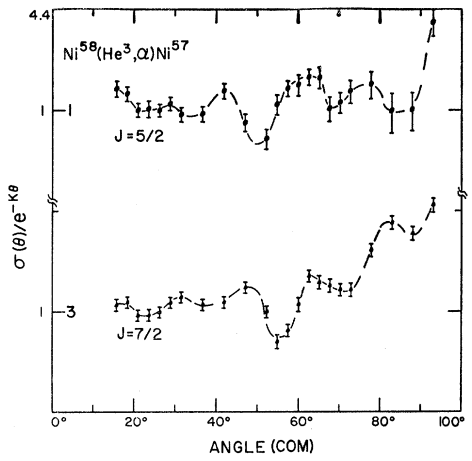

FIG. 16. Center-of-mass plots of the normalized $l=3$, Ni^{58} $(He^3,\alpha)Ni^{57}$ angular distribution. The dashed curves smoothly connect the points.

spectroscopic factors for the first five states in Ni^{59} were required to add up to four. (Two and four are the number of neutrons outside the closed $1f_{7/2}$ shell in each of the Ni^{58} and Ni^{60} targets, respectively.) The results for the normalization factor N are 48.2 for the Ni^{58} target and 44.6 for the Ni^{60} target. The average of these two determinations, $N=46.4$, was used to normalize all of the DWBA calculations. Consequently, for the present (He^3,α) calculations, Eq. (2) reduced to

$$\frac{d\sigma}{d\Omega}=\frac{2S_b+1}{2S_a+1}\frac{N}{(2S_x+1)}S(lj)\bar{\sigma}_{lj}(\theta)=\frac{46.4}{4}S(lj)\bar{\sigma}_{lj}(\theta). \quad (4)$$

$$Ni^{58}(He^3,\alpha)Ni^{57}$$

The DWBA calculations are compared with the $Ni^{58}(He^3,\alpha)Ni^{57}$ angular distributions in Fig. 3. Except for the $l=1$ angular distributions (curves 0 and 2), the fits are good. The general structure of the $l=3$ curves is

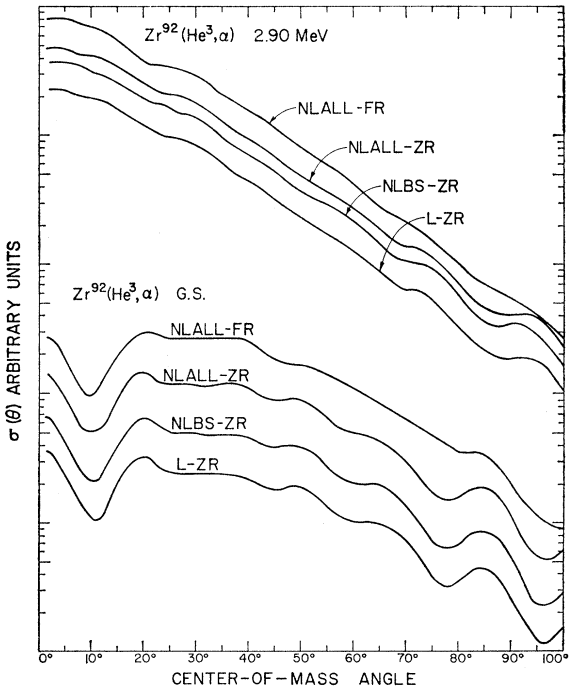

FIG. 17. Comparison of DWBA calculations using four different form-factor options calculated by the program FLANNEL FLURP.

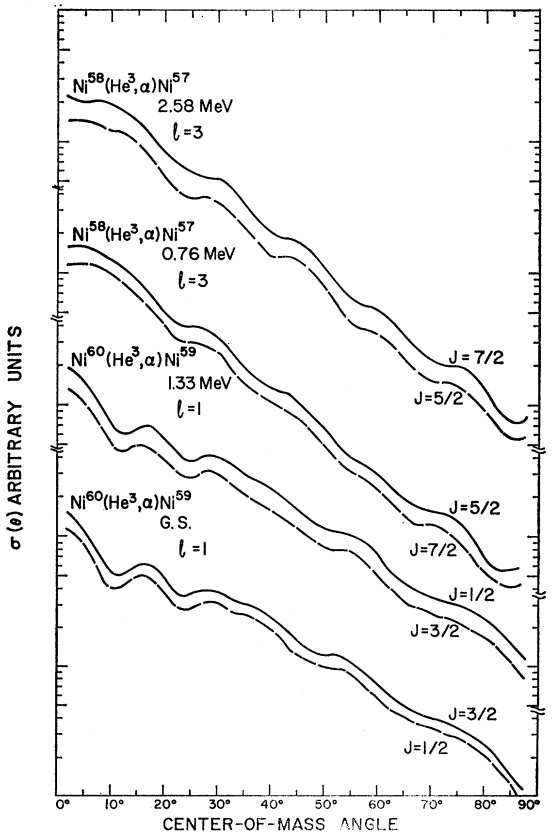

FIG. 18. Comparison of theoretical angular distributions calculated for $J=l\pm\frac{1}{2}$ for $l=3$ and $l=1$.

reproduced in all cases. It is interesting to note that the two most strongly excited $l=3$ angular distributions (curves 3 and 8) show a good resemblance to the theoretical angular distributions. However, the theoretical curve fits the state with the lower Q value (curve 8) somewhat better. The oscillations of the theoretical curve are more pronounced for this level and are in better agreement with the experimental results.

Neither of the theoretical $l=1$ angular distributions show nearly as much structure as the observed angular distributions. The agreement between observed and predicted average slopes is better for curve 2 than for curve 0. It is curious that the transition with the lower Q is again more closely predicted by the DWBA calculations.

It was remarked in Sec. II that experimental angular distributions may have average slopes which depend slightly on the l transfer. Comparing the theoretical $l=1$ angular distributions with those for $l=3$, we see that the $l=3$ curve has a steeper average slope. In fact, the difference in the average slopes of the theoretical curves is more pronounced than has been observed experimentally.

Table I lists the orbital angular-momentum transfer l, the total angular-momentum transfer J, and the spectroscopic factor S for each of the $Ni^{58}(He^3,\alpha)Ni^{57}$ transitions which have been identified. The identification of hitherto unknown l and J is based primarily on the two criteria which were described in Sec. II.

The spectroscopic factor for curve 8, corresponding to an excitation energy of 5.28 MeV in Ni^{57}, deserves a special comment. This state has been identified as the isobaric analog of the g.s. of Co^{57}.[25] A simple formula for the spectroscopic factor has been derived for analog states.[26] (We assume here that all of the strength has been observed in one level.) Following the notation of Sherr *et al.*,[25]

$$S_>=\pi/(N-Z+1), \tag{5}$$

where π is the number of protons outside the inert core, and N and Z are the neutron and proton numbers of the target nucleus. For the Ni^{58} target, for which there are eight protons in the full $1f_{7/2}$ proton shell, $\pi=8$ and $S_>=8/3=2.67$. Our value of $S=2.41$, derived via Ni^{58} and Ni^{60} normalization (Eq. 4), agrees quite well with this number. It is also in agreement with the spectroscopic factor found by Bingham in the $Ni^{58}(He^3,\alpha)Ni^{57}$ reaction at an incident beam energy of 51 MeV.[27] In contrast, Sherr *et al.*[25] found a spectroscopic factor of 1.45 for the $Ni^{58}(p,d)Ni^{57}$ reaction to the analog state.

The sum of all the spectroscopic factors for the $f_{7/2}$ transitions is 8. Adding up the values listed in Table I gives 7.85. This indicates that all, or nearly all, of the strength for the $f_{7/2}$ transitions has been observed in the present experiment.

An interesting feature of the $Ni^{58}(He^3,\alpha)Ni^{57}$ spectrum is that the $f_{7/2}$ excitation strength is split into seven relatively large transitions. This was somewhat unexpected since from a simple picture (neglecting core excitation) one might expect at most three separate $f_{7/2}$ transitions.

$Ni^{60}(He^3,\alpha)Ni^{59}$

Figure 4 illustrates the comparison between the DWBA angular distributions and the measured $Ni^{60}(He^3,\alpha)Ni^{59}$ angular distributions. The general comments made about the predicted DWBA angular distributions for $Ni^{58}(He^3,\alpha)Ni^{57}$ apply in this case as well. The predicted $l=1$ angular distributions (curves 0, 2, and 3) only faintly resemble the experimental data, whereas the predicted $l=3$ angular distributions fit the data reasonably well.

Table II lists the spectroscopic factors along with the angular-momentum quantum numbers for these transitions. Two known states are included in peak 1: a $J=\frac{5}{2}$ level at an excitation energy of 0.34 MeV, and a $J=\frac{1}{2}$ level at an excitation energy of 0.47 MeV. The peak was analyzed as if it were entirely due to an $l=3$ transition.

The sum of the three $f_{7/2}$ spectroscopic factors is 2.28, an indication that in the present experiment we have seen roughly 25% of the total $f_{7/2}$ strength.

$Ni^{61}(He^3,\alpha)Ni^{60}$

Ni^{61} is different than the other Ni isotopes investigated in the present experiment in the sense that the spin of its g.s. is not zero but $\frac{3}{2}^-$. Therefore, the final nuclear spin is not necessarily equal to the total angular-momentum transfer. The transition to the g.s. of Ni^{60} has an extremely small cross section (see Fig. 5). In fact, it is more than one order of magnitude smaller than the cross section for the $Ni^{60}(He^3,\alpha)$ transition to the g.s. of Ni^{59}. A small cross section is expected in view of the configurations of the g.s. of Ni^{61} and Ni^{60}.

The $l=1$ DWBA angular distributions (curves 0 and 1 in Fig. 5) have been normalized rather arbitrarily to the measured angular distributions. The normalization of the DWBA prediction for the transition to the Ni^{60} g.s. was influenced by the fits to the corresponding (He^3,α) angular distributions in Ni^{58} and Ni^{60}. The predicted $l=3$ angular distributions (Fig. 5) are consistent with the experimental results.

Table III lists the $Ni^{61}(He^3,\alpha)Ni^{60}$ transitions that have been identified. Parentheses indicate a tentative assignment. The values for the nuclear spins were taken from the *Nuclear Data Sheets*.[28] Our inability to resolve each of the last three peaks listed in Table III and the

[25] R. Sherr, B. F. Bayman, E. Rost, M. E. Rickey, and C. G. Hoot, Phys. Rev. **137**, B913 (1965).
[26] J. B. French and M. H. Macfarlane, Nucl. Phys. **26**, 161 (1961).
[27] C. R. Bingham (private communication).
[28] *Nuclear Data Sheets*, compiled by K. Way *et al.* (U. S. Government Printing Office, National Academy of Sciences—National Research Council, Washington 25, D. C., 1962).

arbitrary normalization of all curves [Eq. (4)] render tentative our listed spectroscopic factors.

$Ni^{62}(He^3,\alpha)Ni^{61}$

The DWBA angular distributions for the Ni^{62}-(He^3,α)Ni^{61} reactions are compared with the observed angular distributions in Fig. 6. All of the DWBA predictions look reasonable. No clearly resolved $l=1$ angular distributions were found. The transition to the Ni^{61} g.s. has an angular-momentum transfer of $J=\frac{3}{2}$.[29] This transition was not resolved in our experiment from the nearby $J=\frac{5}{2}$ transition. In the DWBA analysis we assumed here only an $l=3$, $J=\frac{5}{2}$ transition, since it has been established that $l=3$ transitions are stronger than $l=1$ transitions. A similar situation exists for the residual level at 1.15 MeV. It is known that there is a $J=\frac{3}{2}$ level in this energy region.[2,29,30] The observed angular distribution resembles the shape of an $l=3$ angular distribution more closely than an $l=1$ shape (see Fig. 6). The experimental data also indicate that the corresponding peak (peak 1) is a multilevel peak. The DWBA analysis assumed that the $l=3$ transition dominated the angular distribution. (The suggestion that both $l=1$ and $l=3$ contribute to peak 1 is consistent with the inelastic scattering analysis presented in the preceding paper.)

The angular distribution for the level at 2.10 MeV (peak 3) is fitted quite well by an $l=4$, $J=\frac{9}{2}$ DWBA prediction. Fulmer and Daehnick[3] suggest the nearby existence of a weak $J=\frac{1}{2}$ level. A weak $l=1$ transition would make a negligible contribution to this angular distribution.

The other three angular distributions that are presented in Fig. 6 appear to correspond to $l=3$, $J=\frac{7}{2}$ transitions. Curve 8 corresponds to several unresolved residual levels and the $l=3$ and $J=\frac{7}{2}$ assignments are therefore tentative.

Since the normalization used to extract the spectroscopic factors was determined from (He^3,α) reactions in Ni^{58} and Ni^{60}, it is probably best to consider the spectroscopic factors listed in Table IV as relative and possibly subject to renormalization.

$Ni^{64}(He^3,\alpha)Ni^{63}$

Observed and predicted angular distributions for the resolved Ni^{64}(He^3,α)Ni^{63} transitions are compared in Fig. 7. The general fits of the DWBA calculations to the experimental angular distributions are similar to those observed for the other Ni isotopes; i.e., the $l=3$ and $l=4$ fits are good, whereas the $l=1$ predictions show only a slight resemblance to the experimental results.

Curve 0 in Fig. 7 shows the typical structureless $l=3$ angular distribution. The weak $l=1$ transition[29] to the ground state of Ni^{63} was not observed. The relatively strong $l=1$ state that Fulmer and Daehnick observe at 0.16 MeV was not completely resolved from the $l=3$ transition. Consequently, the spectroscopic factor listed in Table V for this transition is uncertain.

The DWBA predictions for the $l=1$ transitions (curves 1, 2, and 5) have the same structure as the $l=1$ predictions for the other Ni isotopes. Fulmer and Daehnick observe a weak $l=1$ level at an excitation energy near the peak that we observe at 1.29 MeV. Since this $l=1$ level is weak, its effect on the differential cross section should be negligible. Curves 3 and 6 are closely fitted by $l=4$ DWBA curves.

With the exception of the strong transition to the 0.10-MeV level (peak 0), the most strongly excited group was located at an excitation energy of 3.55 MeV (peak 7). This group and the group located at 4.37 MeV (peak 8) are assigned a spin of $\frac{7}{2}$.

$Zr^{90}(He^3,\alpha)Zr^{89}$

Zr^{90} in the g.s. is usually characterized by a full $g_{9/2}$ neutron shell. The influence of this shell on the (He^3,α) reaction is obvious from the spectrum shown in Fig. 2, in which the α spectrum is seen to be dominated by the transition to the g.s. of Zr^{89}. This transition corresponds to $l=4$; in fact, it is the only $l=4$ transition which we observed for this reaction (see Table VI).

The DWBA predictions are compared with the Zr^{90}(He^3,α)Zr^{89} angular distributions in Fig. 8. The $l=4$ DWBA fit to the strongly excited $g_{9/2}$ transition (curve 0) is only fair. It is somewhat disturbing that the spectroscopic factor extracted from this fit appears to represent only about $\frac{1}{3}$ of the available $g_{9/2}$ strength. This may be due to the use of the normalization obtained from the Ni^{58} and Ni^{60}(He^3,α) reactions. No other strongly excited states were observed in the α spectrum.

Curves 1 and 2 correspond to $l=1$ transitions. The average slope of the predicted curves is not so steep as the average slopes of the experimental curves. Since there is little structure in the observed angular distributions, it is not possible to differentiate between curves with $J=\frac{1}{2}$ and $J=\frac{3}{2}$. The tentative assignment of $J=\frac{1}{2}$ for the first excited state follows from the usual shell-model configuration. Moreover, the extracted spectroscopic factor for the transition to the first excited state is 2.07, a value which exhausts the total strength available for $J=\frac{1}{2}$ transitions. The spectroscopic factor for the $l=1$, $J=\frac{3}{2}$ transition (peak 2) is 2.41.

The angular distributions for the last two peaks (peaks 3 and 4) are predicted reasonably well by $l=3$, $J=\frac{5}{2}$ DWBA curves. The spin assignment of $\frac{5}{2}$ for both these excited states is reasonable, because a $J=\frac{7}{2}$ transition is expected to take place at a much higher excitation energy. The sum of $J=\frac{5}{2}$ spectroscopic

[29] See Ref. 3, and references therein.
[30] R. Sherr, E. Rost, and M. E. Rickey, Phys. Rev. Letters 12, 420 (1964).

factors is 3.67. Our results agree reasonably well with the results of Fou, Zurmuhle, and Joyce.[31]

$$Zr^{91}(He^3,\alpha)Zr^{90}$$

The spin and parity of the g. s. of Zr^{91} is known to be $\frac{5}{2}^+$.[28] The transition to the 0^+ g. s. of Zr^{90} must therefore be due to the pickup of a $d_{5/2}$ neutron. The angular distribution for this $d_{5/2}$ transition along with the angular distributions for three other $Zr^{91}(He^3,\alpha)Zr^{90}$ transitions are shown in Fig. 9. As mentioned in Sec. II, the $d_{5/2}$ angular distributions are the only (He^3,α) distributions in Zr which exhibit a characteristic structure. The DWBA prediction for this transition shows a poor fit to the data. The structure in the theoretical curve only faintly approximates that of the experimental curve. Moreover, as in the $l=1$ case, the average slope of the predicted angular distributions is not as steep as the experimentally observed average slope.

Curve 2 shows an unsuccessful attempt to fit the transition to the level in Zr^{90} at 2.78 MeV with $l=2$. The other two angular distributions shown in Fig. 9 (curves 4 and 5) have the typical steep structureless shape observed in $l=4$ transitions. The magnitude of the cross section and the spectroscopic factors (Table VII) indicate that they both are due to a pickup of a $g_{9/2}$ neutron.

$$Zr^{92}(He^3,\alpha)Zr^{91}$$

Figure 10 illustrates the observed $Zr^{92}(He^3,\alpha)Zr^{91}$ angular distributions and the results of the DWBA calculations. The angular distribution for the transition to the g.s. of Zr^{91} shows the characteristic $l=2$, $J=\frac{5}{2}$ shape. As in the case of the Zr^{91} target, the DWBA prediction for $l=2$ gives a poor fit to the data. Consequently, the extracted spectroscopic factor (Table VIII) is somewhat questionable.

The feeble structure and the average slope of the theoretical ($l=4$) and experimental angular distribution of curve 1 are in accord. Studying (d,t) and (d,p) reactions, Cohen and Chubinsky[4] observed a level near this excitation energy and assigned it $J=\frac{7}{2}$. Our assignment concurs with this result.

Curve 2 represents a strong transition to the level at 2.90 MeV in Zr^{91}. The theoretical curve is for an $l=4$ transition. The experimental data deviate substantially from the theoretical curve.

Peak 3 in the (He^3,α) spectrum from the Zr^{92} target was poorly resolved. Moreover, this transition was weakly excited relative to the transitions to the levels represented by peaks 2 and 4. Consequently, no clear identification of this transition was possible from our data. Cohen and Chubinsky observed an $l=4$, $J=\frac{7}{2}$ transition to an unresolved group at 3.49 MeV. We therefore assumed an $l=4$, $J=\frac{7}{2}$ transition and tried a DWBA fit (see Fig. 10). Although this fit is reasonable, it must be emphasized that the DWBA predictions are not sensitive enough to identify clearly the transition.

As mentioned above, the strong transition (curve 4) at 3.89 MeV was only partially resolved at some angles. Nevertheless, the angular distribution for this transition is consistent with the pickup of a $g_{9/2}$ neutron.

$$Zr^{94}(He^3,\alpha)Zr^{93}$$

The pickup transition to the g.s. is known to correspond to $l=2$.[4] The observed angular distributions and the $l=2$ DWBA predictions for each of these curves are shown in Fig. 11. The shape of the experimental $d_{5/2}$ angular distribution for the transition to the g.s. is consistent with those previously observed in (He^3,α) reactions from Zr^{91} and Zr^{92}. A poor fit of the DWBA prediction to the experimental curve is again seen. Cohen and Chubinsky[4] and Schiffer *et al.*[32] have presented evidence that the group which we observe at 1.49 MeV should correspond to a $d_{3/2}$ transition. However, the predicted $l=2$ angular distribution shows little resemblance to our experimental curve, and no assignment can be suggested here.

The other three angular distributions presented in Fig. 11 indicate by their average slopes that they correspond to an $l=4$ transition. The relatively weak transition to the group at 2.05-MeV excitation should be due to the pickup of a $g_{7/2}$ neutron. The fit of the DWBA prediction is consistent with an $l=4$ assignment. The strongly excited transitions (curves 3 and 4) are expected to be due to a pickup of $g_{9/2}$ neutrons. These assignments (Table IX) are based on their strength in our pickup reaction and their absence in the $Zr^{92}(d,p)Zr^{93}$ stripping reactions.

In Fig. 11 we also plotted DWBA predictions that were calculated in the L-ZR for the last three $l=4$ angular distributions. It is noteworthy that the NLALL-FR DWBA predictions follow more closely the experimental results at the larger angles. The reason for this is possibly due to the greater momentum transfer at the larger angles.[33] In other words, effects, such as the finite-range of the interaction, become more important for larger momentum transfer.

The sum of the spectroscopic factors for the $g_{9/2}$ transitions is 1.96. This is small compared to the total available strength. However, a large α background was observed in the $Zr^{94}(He^3,\alpha)Zr^{93}$ spectra at excitation energies greater than 4 MeV. It is conceivable that the $g_{9/2}$ strength is divided among many states above 4 MeV.

V. SUMMARY AND CONCLUSIONS

Using the LEA, we have attempted to improve upon the "standard" L-ZR DWBA calculations for (He^3,α)

[31] C. M. Fou, R. W. Zurmuhle, and J. M. Joyce, Phys. Rev. **155**, 1248 (1967).

[32] J. P. Schiffer, L. L. Lee, Jr., A. Marinov, and C. Mayer-Boricke, Phys. Rev. **147**, 829 (1966).

[33] R. M. Drisko (private communication).

reactions. For $l=1$ and $l=2$ transitions, the disagreements between theoretical and experimental angular distributions were not substantially improved. However, for $l=3$ and $l=4$ transitions, the predictions were in reasonable agreement with the observed angular distributions. In particular, the observed discrepancies in the L-ZR angular distributions at the larger angles were essentially removed in the NLALL-FR calculations.

As noted in the discussion of the $Ni^{58}(He^3,\alpha)Ni^{57}$ reactions, the predicted DWBA angular distributions seem to be somewhat Q-dependent. Therefore, the agreement of the DWBA curve with the experimental curve was also slightly Q-dependent. The momentum transfer increases with increasing Q value, and thus properties which depend on the momentum transfer, such as the finite range of the interaction, are expected to increase in importance.[15] This implies that the LEA's only partially correct for these effects. This may also partially explain the disagreement with experiment of the $l=1$ and $l=2$ predictions, because these transitions usually have large Q values.

We found that (He^3,α) angular distributions exhibited some J-dependence effects[34] for neutron pickup from $2p$ and $1f$ orbits. Oscillatory structure was observed for $l=1$ transitions. The oscillations were more pronounced for $J=\frac{3}{2}$ than for $J=\frac{1}{2}$. For $l=3$ angular distributions, the degree of structure was similar for both $J=l\pm\frac{1}{2}$, but the prominent features of the $J=\frac{5}{2}$ angular distribution occurred approximately 5 deg forward of similar features in the $J=\frac{7}{2}$ angular distribution. No J dependence could be observed for $l=2$ and 4.

Suggested assignments for the orbital angular-momentum transfer (l) and the nuclear spin of the residual nucleus (J) are listed in Tables I–IX. Where possible, the listed assignments were compared with previous experimental results. The newly assigned l and J values for transitions that have not been previously observed are based primarily on the shape and average slope of the experimental angular distributions. The experimental energy resolution was limited ($\approx$140 keV). Since some of the transitions were weak, several l and J assignments are given with reservations.

The accuracy of the extracted spectroscopic factors S listed in Tables I–IX is also subject to the above uncertainties. In addition, it depends on the theoretical uncertainties of the DWBA theory and the normalization of the predicted angular distributions to the experimental curves. The absolute values listed for S must therefore be considered only as rough approximations, with more weight being attached to the relative S values within a single isotope.

As to the question of whether or not the (He^3,α) reaction is a good spectroscopic tool, we wish to suggest the following concluding observations. Our experiment represents an attempt to answer this question for medium-A nuclei, medium-He^3 energy (25 MeV), and moderate energy resolution. We developed several operational criteria which enabled us to suggest a few spectroscopic assignments, but often encountered difficulties in the determination of angular momenta. The consistency of our results, and the general agreement with previous assignments, when data are available, are gratifying. However, the whole procedure should only be regarded as suggestive, mainly due to the moderate agreement with theory and to the absence of rigorous and more objective criteria. We therefore conclude that the (He^3,α) reaction is, at present, only of limited spectroscopic value. This is unfortunate in view of the high Q value of these reactions, and their enhanced importance relative to (p,d) or (d,t) reactions whenever large l transfers are involved.

We believe that more extensive investigations with better energy resolution as well as more reliable optical-model parameters and a more refined model are desirable. Only after such improvements are realized would it be possible to make a final judgment on the spectroscopic worth of the (He^3,α) reaction.

ACKNOWLEDGMENTS

We would like to thank the Oak Ridge Associated Universities for the use of their computer facilities. We would particularly like to thank C. R. Bingham for his hospitality, and his invaluable assistance and guidance with the DWBA analysis. We wish also to thank R. M. Drisko for his help with the DWBA analysis and for several informative discussions. One of us (D.E.R.) would like to acknowledge the financial support of an Atomic Energy Commission Fellowship from the Oak Ridge Institute of Nuclear Studies during the initial period of this experiment. We also thank L. E. Ernest and the cyclotron staff for their cooperation in this experiment.

[34] For a comprehensive discussion, see C. Glashausser and M. E. Rickey, Phys. Rev. **154**, 829 (1967).